

Electronic Supporting Information

Hierarchical Porous Metallized Poly-melamine-formaldehyde(PMF) as Low-Cost and High-Efficiency Catalyst for Cyclic Carbonate Synthesis from CO₂ and Epoxide

^a Jian Yin, ^aTianqi Zhang, ^bEmily Schulman, ^bDongxia Liu, ^aJianqiang Meng*

^a State Key Laboratory of Separation Membranes and Membrane Processes, Tianjin Polytechnic University, Tianjin 300387

^bDepartment of Chemical and Biomolecular Engineering in University of Maryland at College Park, Maryland 20742

Correspondence and requests for materials should be addressed to Jianqiang Meng (email: jianqiang.meng@hotmail.com)

Content

General experimental methods.....	4
Materials	4
Instrumentation	4
Fabrication of ah-PMF particles	4
Fabrication of CE-1 and CE-2 particles	4
Metallization of ah-PMF particles	5
Cycloaddition of CO ₂ with epoxide catalyzed by Zn@ah-PMF.....	5
Prediction of the selectivity of CO ₂ /N ₂ mixtures by IAST	5
DFT calculations:	6
General Characterization of Zn@ah-PMF.....	7
Fig S1 Photographs of non-aqueous HIPES	7
Fig. S2 Photograph of the ah-PMF monolith.....	8
Fig. S3 FT-IR spectrum of Zn@ah-PMF.....	9
Fig. S4 Solid ¹³ C NMR spectra of Zn@ah-PMF.....	10
Fig. S5 XPS spectra of ah-PMF and Zn@ah-PMF.....	11
Scheme S1 The repeating unit of the ah-PMF polymer and the ideal molecular structure diagram of Zn@ah-PMF	12
Fig. S6 EDX mapping of Zn@ah-PMF.....	13
Table S1 The EDX elemental quantitative analysis of Zn@ah-PMF	14
Fig. S7 Thermal gravimetric analysis (TGA) on Zn@ah-PMF under nitrogen atmosphere.....	15
Fig. S8 Adsorption and desorption isotherms of N ₂ at 77 K and pore size distribution curve of Zn@CE-1 and Zn@CE-2	16
Fig.S9 SEM and TEM images of Zn@CE-1 and Zn@CE-2.....	14
Fig. S10 The XRD patterns of Zn@CE-1, Zn@CE-2, and Zn@ah-PMF samples.....	15
Fig. S11 SEM image of Zn@ah-PMF with a particle size of 400 mesh.....	16
Fig. S12 BET plot (P/P ₀ =0.06-0.2) from N ₂ isotherms at 77 K of Zn@ah-PMF.....	17
Table S2 The stability of HIPES at different conditions	18
Fig. S13 The fitted adsorption isotherms of CO ₂ and N ₂	19
Table S3 A summary of CO ₂ capacities and BET surface areas of other catalysts reported in literature.....	20
Catalytic results.....	21
Scheme S2 The proposed reaction mechanism of PO with CO ₂ catalyzed by Zn@ah-PMF.....	21
Fig. S14 The TOF, TON and conversion of the cycloaddition reaction of PO and CO ₂ at 25 °C and 0.1 MPa.....	22
Fig. S15 The SEM image of Zn@ah-PMF sample after 55 h catalytic reaction.....	23
Fig. S16 The recyclability tests of Zn@ah-PMF.	24
Table S4 Cycloaddition reaction of epoxides with CO ₂	25
Fig. S17 Typical ¹ H NMR method used to calculate the yield of PO.....	26
¹ H NMR spectra of the products	27
Table S5 Comparison of the Zn@ah-PMF catalyst with the reported catalysts.....	30
Reference (1-40: main text references, 41-82: electronic supporting information references)..	32
Appendix 1 The program code of IAST	34
Appendix 2 The input value and the predicted results of ideal gas and flue gas via IAST	36

General experimental methods.

Materials

Melamine (99%) was purchased from J&K Scientifics Ltd. (Beijing, China). Pluronic F127 was purchased from Sigma-Aldrich Co., LLC. (Shanghai, China). Isopar M was purchased from Exxon Mobil Co., Ltd. Paraformaldehyde (AR), propylene oxide (99%), tetrabutylammonium bromide (AR, 99%), Zinc chloride (AR), Epichlorohydrin (AR). Styrene oxide (AR), Allyl glycidyl ether (AR) and Chloroform-d (D, 99.8%) with 0.03% v/v TMS were purchased from Aladdin Bio-Chem Techno. Co., Ltd. Ethylenediaminetetraacetic acid disodium salt dihydrate (EDTA-2Na, AR), Ammonium chloride (AR), Hydrochloric Acid (AR), Eriochrome Black T (AR), Methyl Alcohol (AR) and other chemicals were purchased from Tianjin Kermel Chemical Reagent Co., Ltd. Deionized water (DI water, 18.2 MΩ cm at 25 °C, 1.2 µg/L TOC) was obtained from a Millipore Milli-Q Advantage A10 water purification system (Billerica, MA, USA). All the chemicals were used without further purification.

Instrumentation

FT-IR spectra were recorded on a Thermo Scientific Nicolet iS50 FT-IR spectrometer at the resolution of 0.09 cm⁻¹. X-ray photoelectron spectroscopy (XPS) spectra were collected on a Thermo Scientific K-Alpha XPS spectrometer. Liquid ¹H NMR spectra were recorded on a Bruker 400 spectrometer. Solid ¹³C NMR spectra were recorded on a 500 MHz Avance Solids NMR. The CDCl₃ with TMS was used as an internal reference, and the residue H peaks of CHCl₃ were at 7.26 ppm. The N₂ adsorption and desorption isotherms were measured by a Micromeritics ASAP 2020M system at 77 K. The samples were deaerated at 120 °C for 8 h before measurements. The specific surface area was calculated by the Langmuir and the Brunauer-Emmett-Teller (BET) methods. The pore size distribution curve was calculated by using the non-local density functional theory (NLDFT) method. The XRD pattern was measured by a BRUKER D8 DISCOVER X-ray Powder Diffractometer. The field emission scanning electron microscopy (FE-SEM) measurement was carried out on a Zeiss Gemini SEM 500 microscope. The high-resolution transmission electron microscopy (HR-TEM) images were obtained by a JEOL JEM-2100F. The TGA measurement was carried out on a Q600 Simultaneous DSC-TGA over the temperature range of 25 °C to 800 °C under a N₂ atmosphere. The catalytic reaction was conducted in a stainless-steel autoclave (SLM Micro-Reactor, Beijing Century Senlong Co., Ltd.) with a 25 mL Teflon tube.

Fabrication of ah-PMF particles

Firstly, Pluronic F127 (4.62 g) and DMSO (12 mL) were placed in a three-neck flask (250 mL) and dissolved at 70 °C for 1 hour. Then, melamine (MA, 1.134g, 9 mmol) and paraformaldehyde (PF, 0.486 g, 16.2mmol) were added and dissolved at 95 °C for another 2 hours. Subsequently, Isopar M (40 mL) was added dropwise into the resulting solution with constant mechanical stirring at the speed of 120-150 rpm at 45 °C, until no phase separation was observed. The resulting creamy emulsion was poured into a hydrothermal reactor and heated at 170 °C for 3 days in an oven. After polymerization, the solid sample was stirred and washed using the solvents acetone, THF, and water successively. Finally, the solid powder was dried in a vacuum oven at 120 °C for 24 h. The yield of PMF product was 91.6%.

Fabrication of CE-1 and CE-2 particles

For the CE-1 sample, melamine (MA, 1.134g, 9 mmol), paraformaldehyde (PF, 0.486 g, 16.2mmol) and DMSO (12 mL) were placed in a three-neck flask (250 mL) and dissolved at 70 °C for 1 hour. The mixed solution was poured into a hydrothermal reactor and heated at 170 °C for 3 days in an oven. For the CE-2 sample, Pluronic F127 (4.62 g) and DMSO (12 mL) were placed in a three-neck flask (250 mL) and dissolved at 70°C for 1 hour. Melamine(MA, 1.134g, 9 mmol) and paraformaldehyde (PF, 0.486 g, 16.2mmol) were added and dissolved into the mixed solution. The resulting solution was poured into a hydrothermal reactor and heated at 170 °C for 3 days in an

oven. After polymerization, the washing processes for these two samples was the same as the washing process used for the ah-PMF particles.

Metallization of ah-PMF particles

The metallization of ah-PMF particles was carried out via stirring in a 0.1 M ZnCl₂ solution for 24 h, followed by filtration and drying in a vacuum oven at 120 °C for 12 h. The Zn ion uptake was characterized by the titration method using EDTA as the titrant. Specifically, 3 mL of ammonium chloride buffer solution (pH=10) and one drop of Eriochrome Black T solution (0.5 g EBT in 75 mL of triethanolamine and 25 mL of ethanol) were mixed into 9 mL of filtrate. Then, 0.1 M EDTA solution was added dropwise into the mixed solution until the color of solution changed from purple to blue. The concentration of Zn ions was calculated via Eq. (1):

$$c_{Zn^{2+}} = \frac{c_{EDTA} \cdot (V_1 - V_2)}{V} \quad (1)$$

where c_{EDTA} is the concentration of EDTA solution, V is the volume of the filtrate, V_1 is the volume of EDTA solution used to titrate the filtrate, and V_2 is the volume of EDTA solution used for titrating the same volume of control solution, which is usually water. The Zn ions uptake was calculated via Eq. (2):

$$m_{Zn^{2+}} = \frac{\Delta c_{Zn^{2+}} \cdot V_0 \cdot M_{Zn}}{m_{PMF}} \quad (2)$$

where $\Delta c_{Zn^{2+}} = c_{Zn_1^{2+}} - c_{Zn_2^{2+}}$ is the change of the concentration of Zn ions, V_0 is the initial volume of ZnCl₂ solution, M_{Zn} is the molecular weight of Zn, and m_{PMF} is the mass of PMF particles.

Cycloaddition of CO₂ with epoxide catalyzed by Zn@ah-PMF.

First, the autoclave was purged with CO₂ to evacuate air for 10 min. Then, Zn@ah-PMF particles (16 mg, 0.0085 mol%), propylene oxide (15 mL, 214.3 mmol), and TBAB (464 mg) were added into the reactor. After charging CO₂ up to 2 MPa, the reactor was stirred at 100 °C for 0.5 h. When the reaction was finished, the resident CO₂ was vented at room temperature. The product yield was calculated by ¹H NMR (CDCl₃) with 1,1,2,2-tetrachloroethane as an internal standard. For the recyclability test, the catalyst was filtrated, washed with methanol for 4 times, and then vacuum dried at 120 °C for 24 h for the next recycling use.

Prediction of the selectivity of CO₂/N₂ mixtures by IAST

IAST (ideal adsorption solution theory) is a widely used method to predict binary mixture adsorption from the experimental results of pure-gas isotherms.⁴¹⁻⁴³ Firstly, the pure-gas isotherms should be well fitted by a proper adsorption model. Here, we used the following adsorption models to fit the isotherms of CO₂ and N₂.

1) Single-site Langmuir equation (SSL)

$$q = \frac{q_m bp}{1 + bp} \quad (3)$$

where p is the pressure of the bulk gas at equilibrium (MPa), q is the adsorbed amount per mass of adsorbent (mmol/g), q_m is the saturation capacity of adsorbent, and b is the affinity coefficient.

2) Dual-site Langmuir equation (DSL)

$$q = \frac{q_{m,1}b_1p}{1+b_1p} + \frac{q_{m,2}b_2p}{1+b_2p} \quad (4)$$

where the parameters are the same as in the SSL equation. The subscript 1 and 2 stand for sites 1 and 2, respectively.

3) Single-site Langmuir-Freundlich equation (SSLF)

$$q = \frac{q_m bp^{1/n}}{1+bp^{1/n}} \quad (5)$$

where n is the deviation from an ideal homogenous surface. Other parameters are the same as in the SSL equation.

4) Dual-site Langmuir-Freundlich equation (DSLF)

$$q = \frac{q_{m,1}b_1p^{1/n_1}}{1+b_1p^{1/n_1}} + \frac{q_{m,2}b_2p^{1/n_2}}{1+b_2p^{1/n_2}} \quad (6)$$

where the parameters used are the same as in the SSLF equation, and the subscript 1 and 2 stand for sites 1 and 2, respectively.

The results shown in Fig. S10 indicate that the dual-sites Langmuir-Freundlich (DSLF) equation is the most suitable model ($R^2=0.99998$), which was then used to predict the selectivity of mixtures based on IAST. The selectivity of mixtures is defined as:

$$S_{A/B} = \left(\frac{x_A}{x_B} \right) \left(\frac{y_B}{y_A} \right) \quad (7)$$

where x and y are the mole fractions of the components in the adsorbed and bulk phases, respectively. The subscript A and B represent the components of the mixtures, which stand for CO₂ and N₂ here. We utilized Fortran language to calculate selectivity and the program code is shown in Appendix I.

DFT calculations:

The Density functional theory (DFT) calculations of the molecular structure of ah-PMF polymer were performed by using Materials Studio software with DMol3 DFT module at the B3LYP level.^{81,82}

General Characterization of Zn@ah-PMF

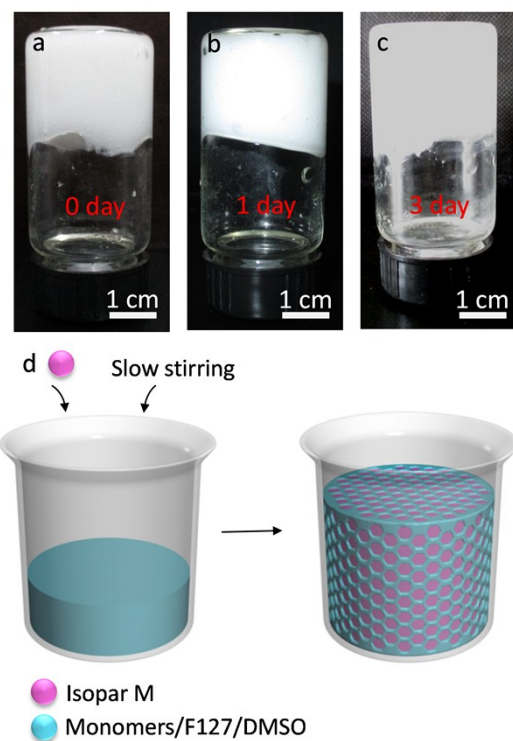


Fig S1 Photographs of non-aqueous HIPE with different preservation times at room temperature (a-c) and its structure diagram (d).



Fig. S2 Photograph of the ah-PMF monolith.

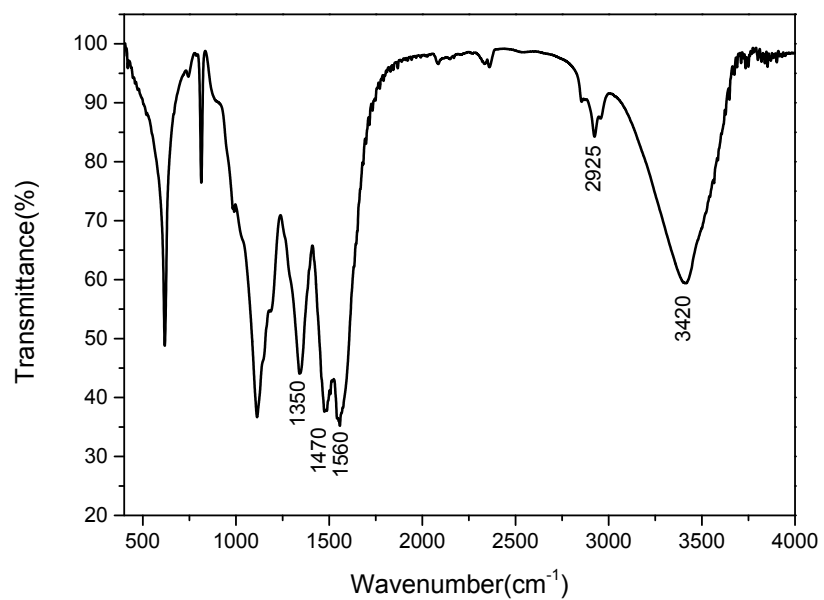


Fig. S3 FT-IR spectrum of Zn@ah-PMF.

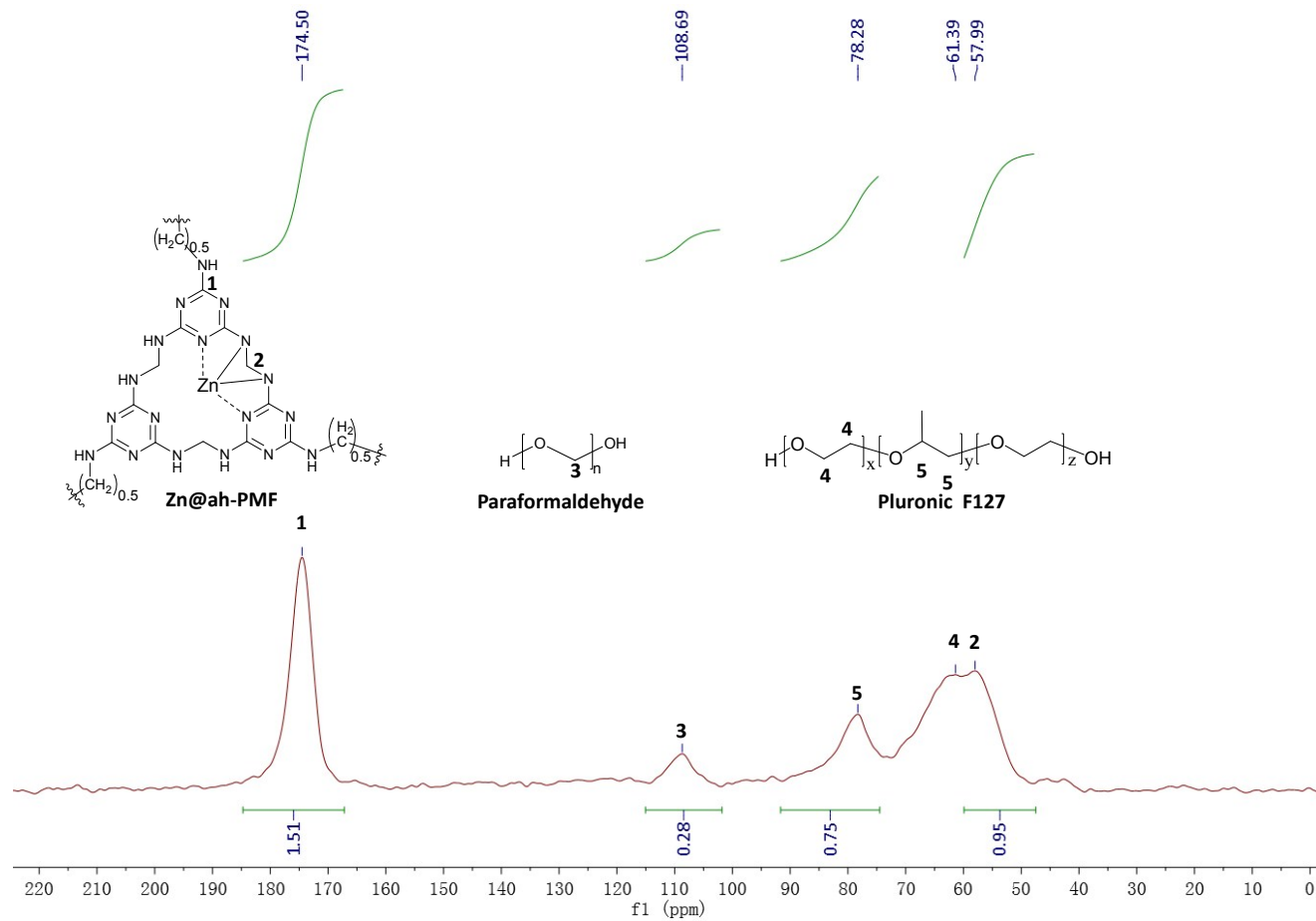


Fig. S4 Solid ^{13}C NMR spectra of Zn@ah-PMF

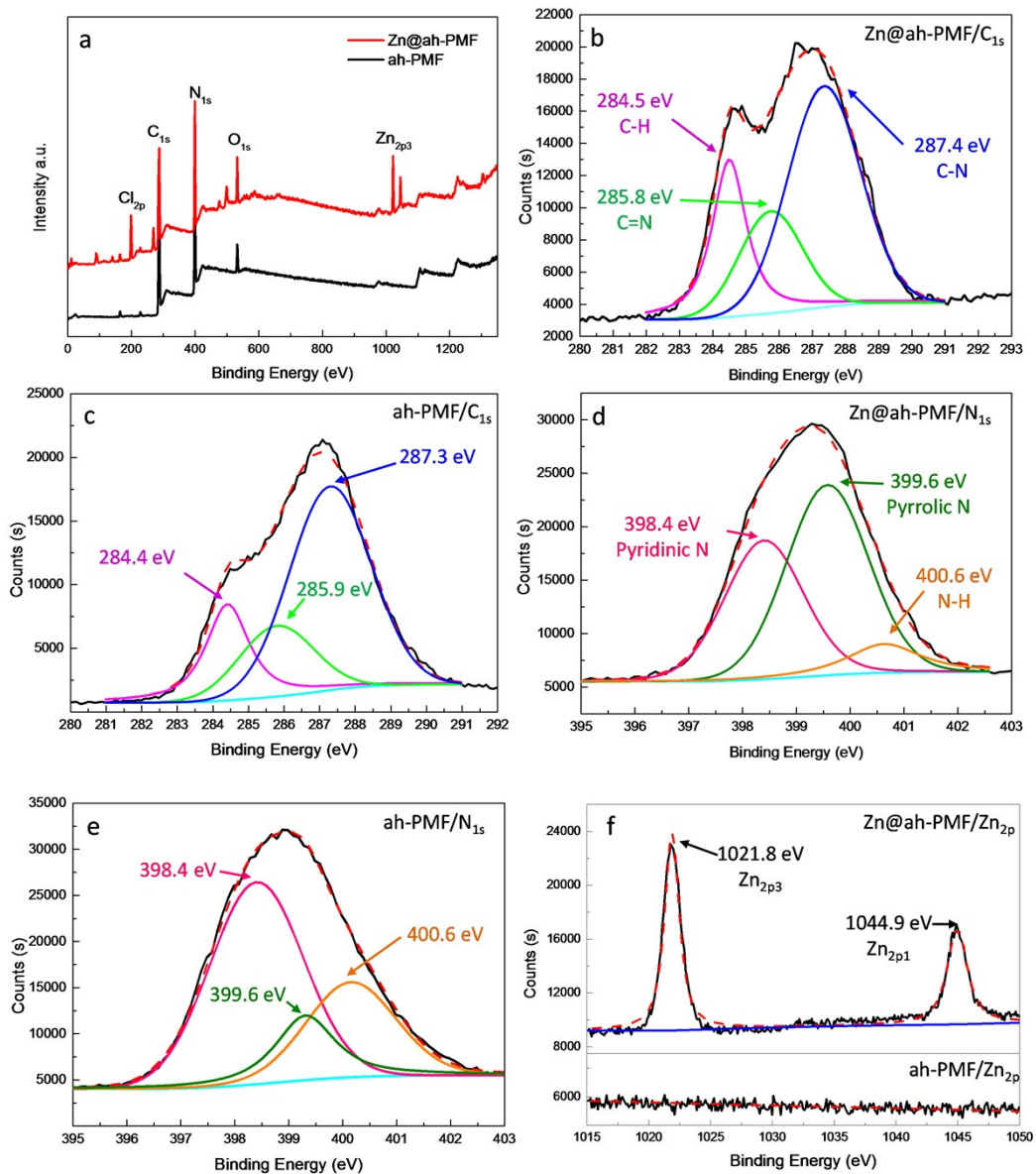
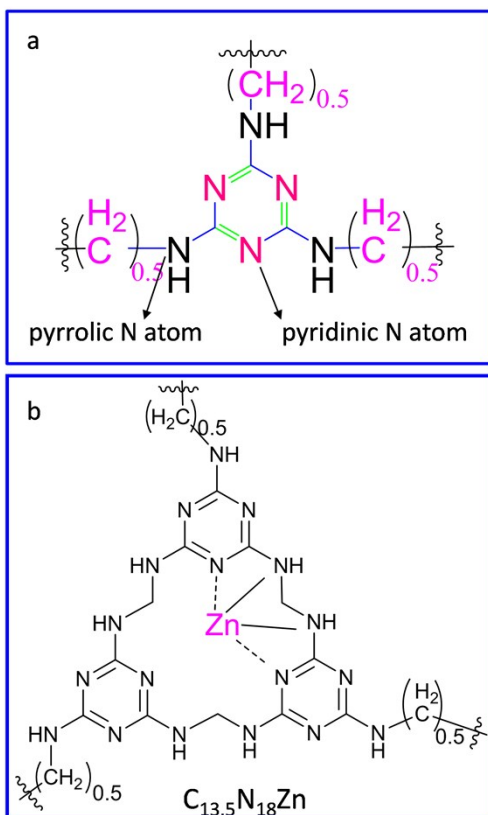


Fig.S5 XPS spectra of ah-PMF and Zn@ah-PMF.



Scheme S1 (a) The repeating unit of the ah-PMF polymer. (b) The ideal molecular structure diagram of Zn@ah-PMF

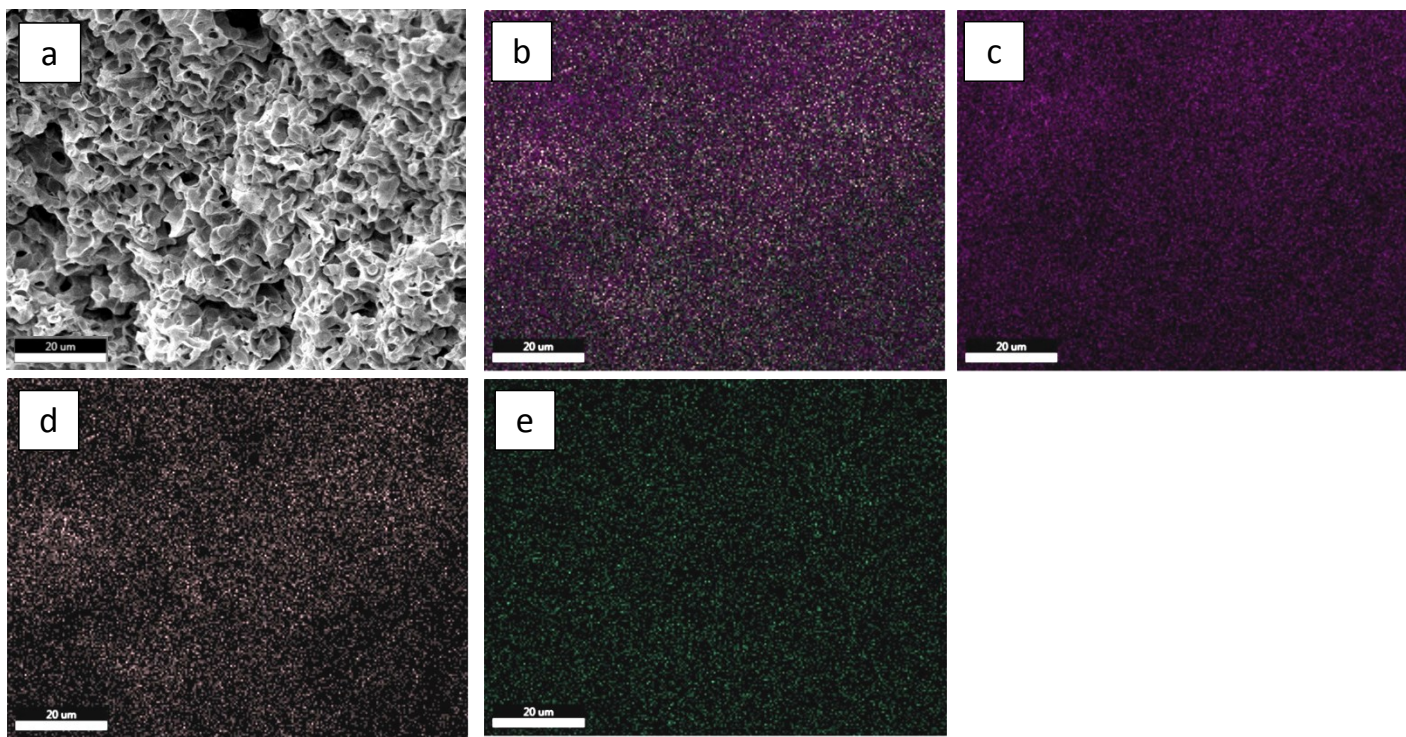


Fig. S6 EDX mapping of Zn@ah-PMF: (a) SEM image and (b) EDS layered image of Zn@ah-PMF, in which the colors purple, brown, and green represent elements C, N and Zn, respectively. (c)-(e) The images of element mapping of C, N and Zn.

Table S1 The EDX elemental quantitative analysis of Zn@ah-PMF

Element	Weight %	Atomic %	Error %
C K	37.88	45.29	6.49
N K	50.97	52.26	10.34
ZnK	11.15	2.45	3.32

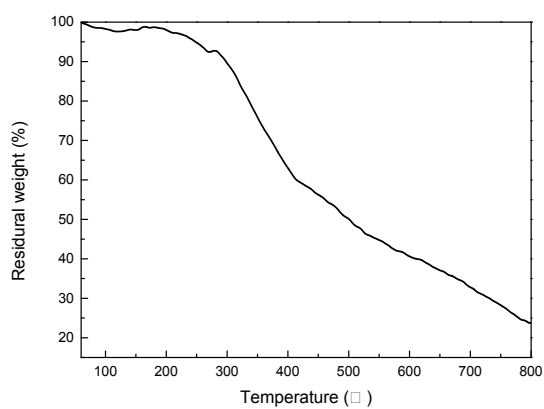


Fig. S7 Thermal gravimetric analysis (TGA) on Zn@ah-PMF under nitrogen atmosphere

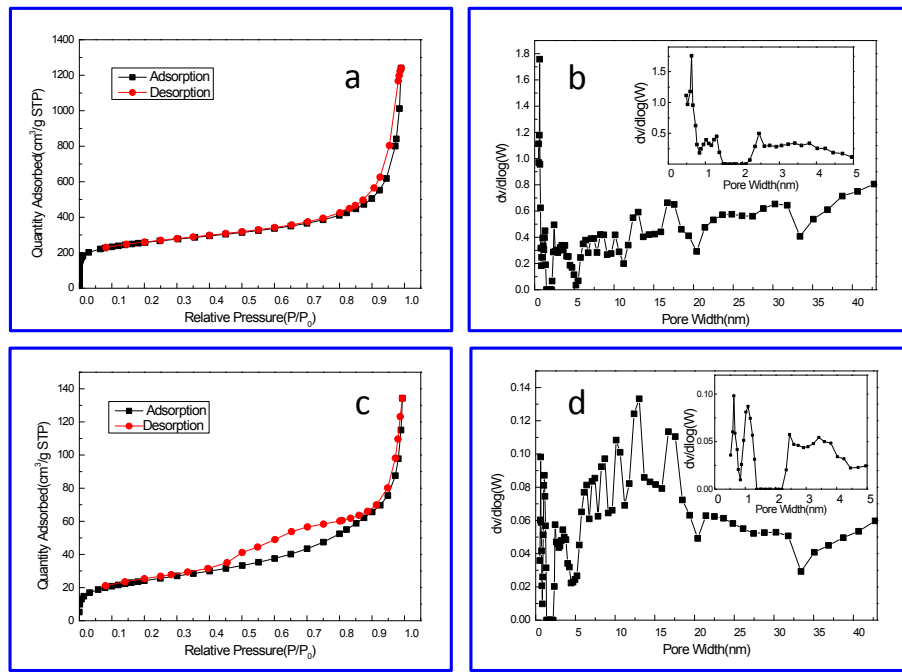


Fig. S8 (a) Adsorption and desorption isotherms of N₂ at 77 K of Zn@CE-1; (b) Pore size distribution curve of Zn@CE-1; (c) Adsorption and desorption isotherms of N₂ at 77 K of Zn@CE-2; (d) pore size distribution curve of Zn@CE-2

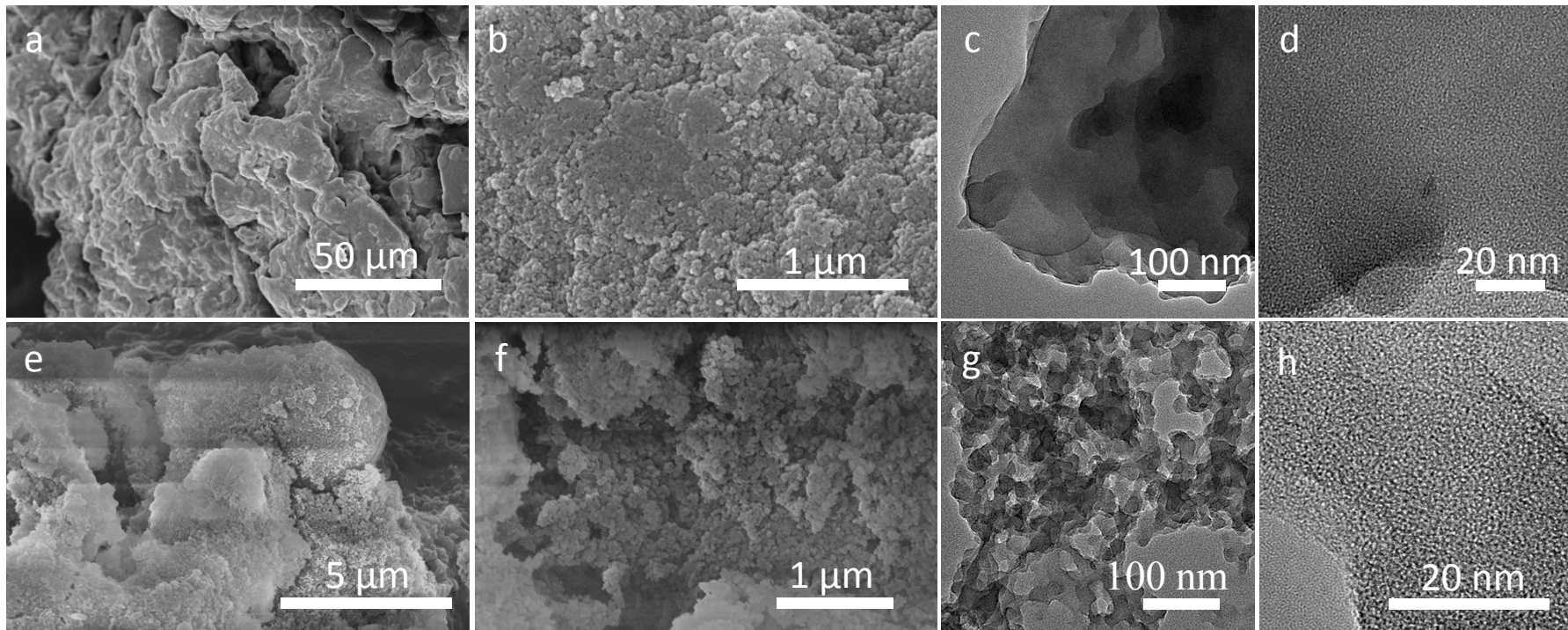


Fig.S9 SEM and TEM images of Zn@CE-1 (a-d) and Zn@CE-2 (e-h).

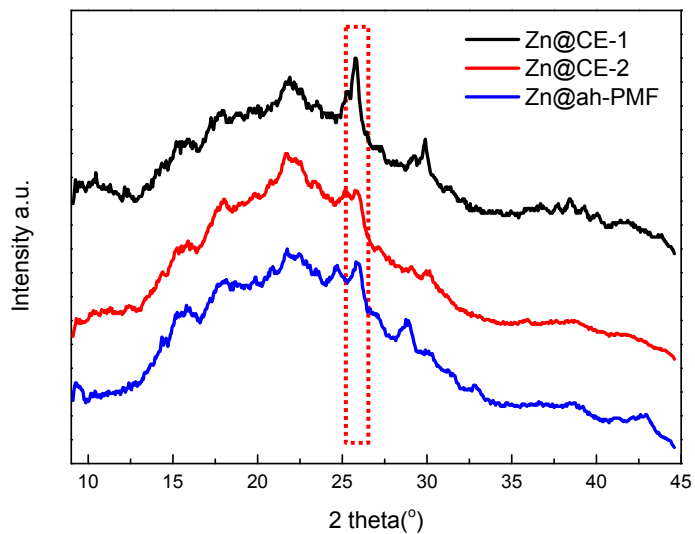


Fig. S10 The XRD patterns of Zn@CE-1, Zn@CE-2, and Zn@ah-PMF samples.

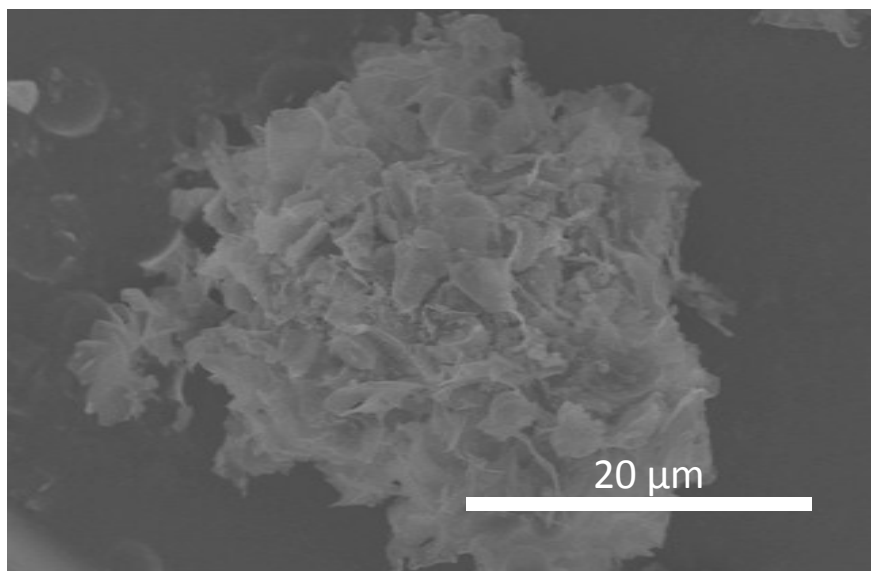


Fig. S11 SEM image of Zn@ah-PMF with a particle size of 400 mesh.

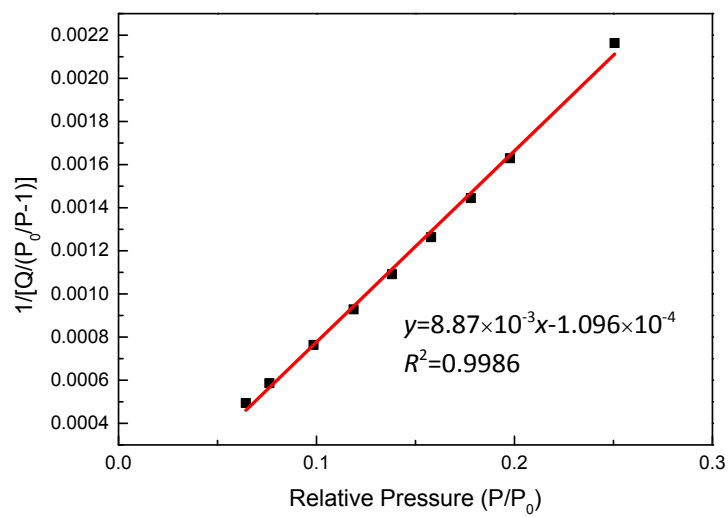


Fig. S12 BET plot ($P/P_0=0.06-0.2$) from N_2 isotherms at 77 K of Zn@ah-PMF.

Table S2 The stability of HIPEs at different conditions.

Dispersed phase/Temp. (°C)	75	85	120	140	160
Petroleum ether (b.p. 60-90 °C) at 1 atm	boiling	-	-	-	-
Petroleum ether (b.p. 90-120 °C) at 1 atm	phase separation	boiling	-	-	-
Isopar M at 1 atm	stable	stable	stable	phase separation	boiling
Isopar M in hydrothermal reactor	stable	stable	stable	stable	stable

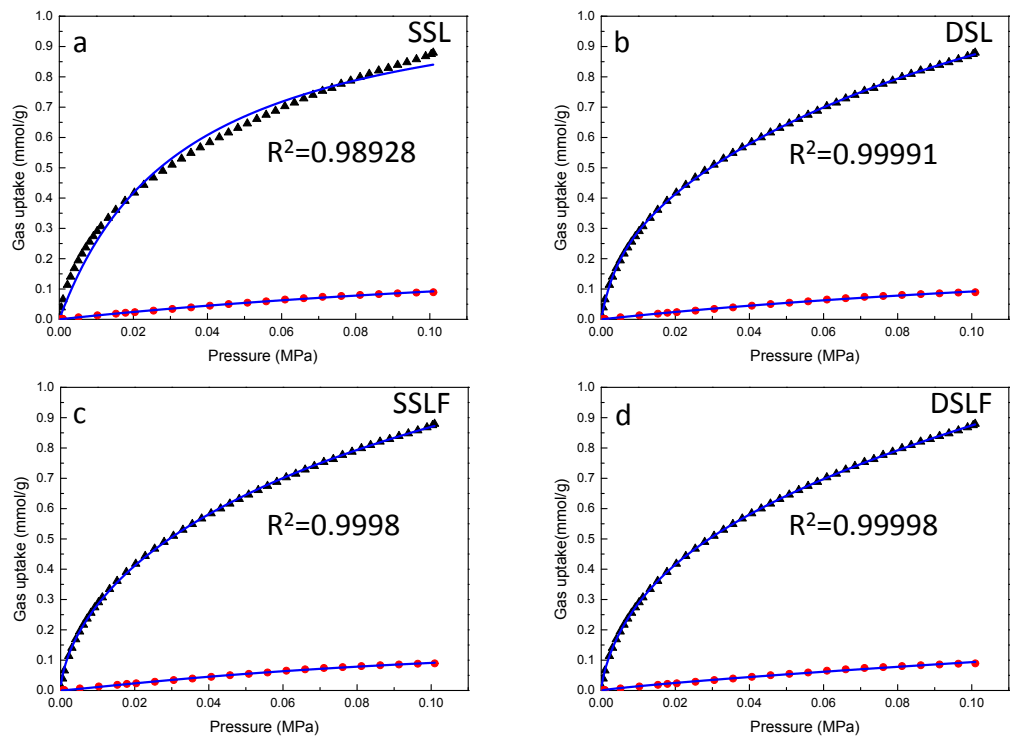
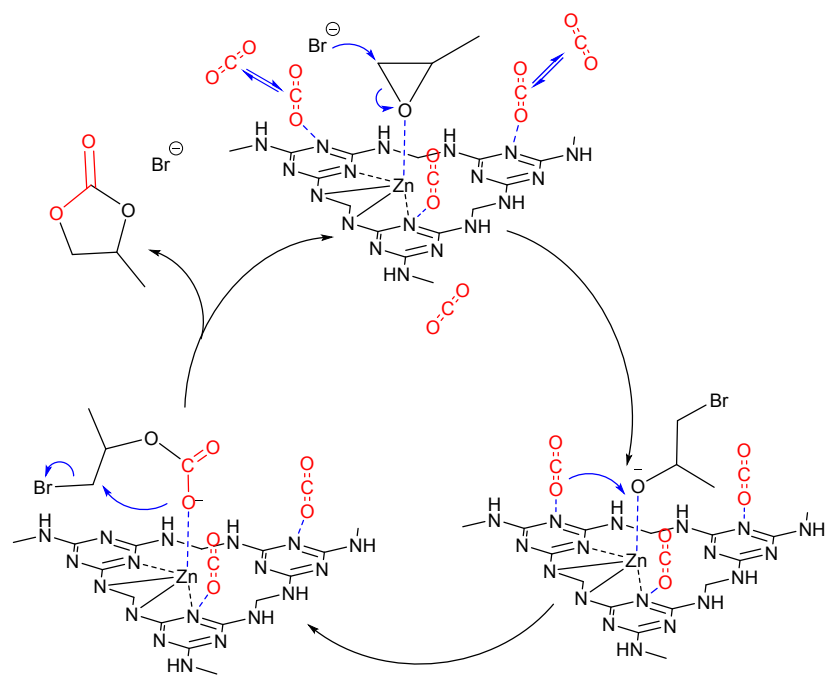


Fig. S13 The fitted adsorption isotherms of CO₂ (blue triangles) and N₂ (red dots) via (a) SSL, (b) DSL, (c) SSLF and (d) DSLF models.

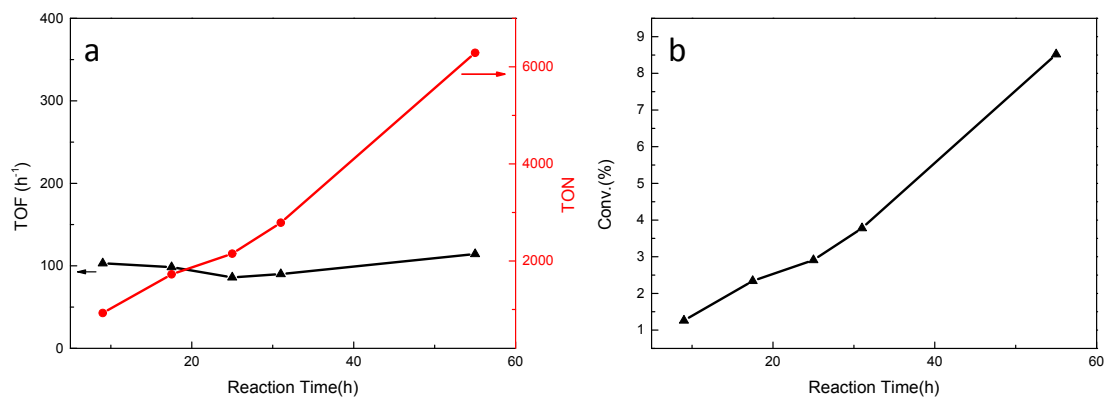
Table S3 A summary of CO₂ capacities and BET surface areas of other catalysts reported in literature.

Catalyst	Temp.[°C]	CO ₂ capacity (mg/g)	BET surface area (S _{BET})	Ref.
Co-CMP	25	79.3	965	11
Zn-CMP	25	58.4	791	52
PPh ₃ -ILBr-ZnBr ₂ @POPs	25	31.5	482	13
Al-HCP	0	93.3	400	78
Al-CMP	0	43.1	1278	80
HUST-1-Co	0	213.9	1360	15
Py-Zn@MA	0	58.1	207	22
Bp-Zn@MA	0	52.37	445	21
Zn/HAzo-POP-2	0	53.3	593.48	18
Cu/POP-Bpy	0	129	683	20
ah-PMF	0	38.3	497	This work

Catalytic results.



Scheme S2 The proposed reaction mechanism of PO with CO_2 catalyzed by $\text{Zn}@\text{ah-PMF}$.



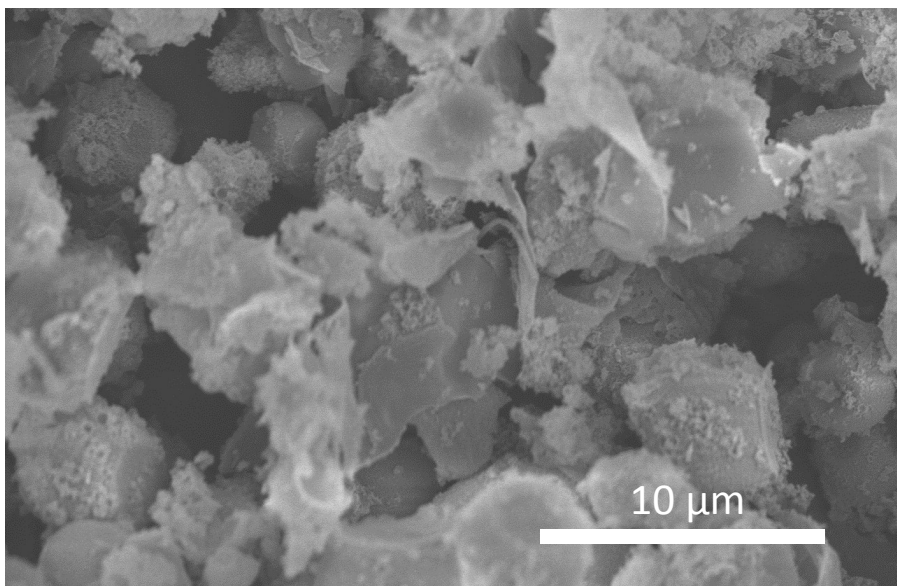


Fig. S15 The SEM image of Zn@ah-PMF sample after 55 h catalytic reaction.

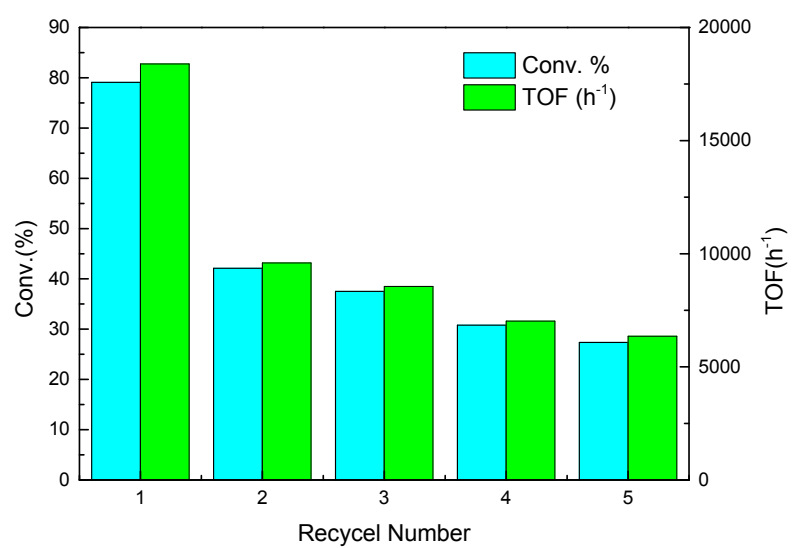


Fig. S16 The recyclability tests of Zn@ah-PMF.

Table S4 Cycloaddition reaction of epoxides with CO₂^[a].

Entry	Epoxides	Produces	Conv.[%] ^[b]	TOF[h ⁻¹] ^[c]
1 ^[d]			87.9	14473
2 ^[e]			51.8	10151
3 ^[f]			80.3	17698

[a] Reaction conditions: Epoxides, Zn@ah-PMF (16 mg), TBAB (0.414 g), the initial pressure of CO₂ is 2 MPa, 100 °C and 0.5 h. [b] Determined by ¹H NMR spectroscopy (CDCl₃, 400 MHz) using 1,1,2,2-tetrachloroethaneas as an internal standard. [c] TOF=[moles of product]/[(total moles of metal ions)*(reaction time)]. [d] Epichlorohydrin (18.3 mL, 233 mmol). [e] Allyl glycidyl ether (25.3 mL, 213.4 mmol). [f] 1,2-Epoxyethylbenzene (24.5 ml, 214 mmol).

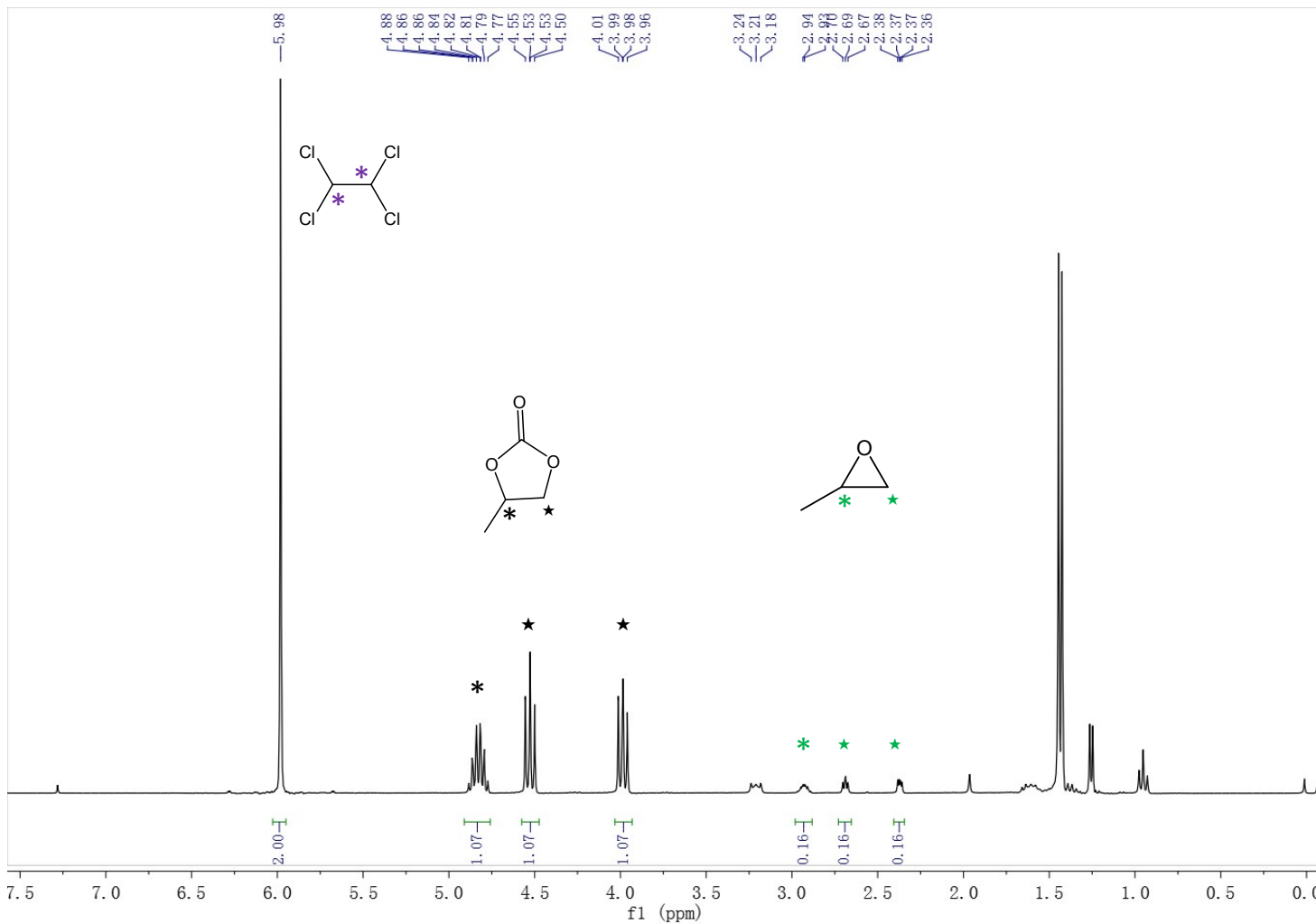
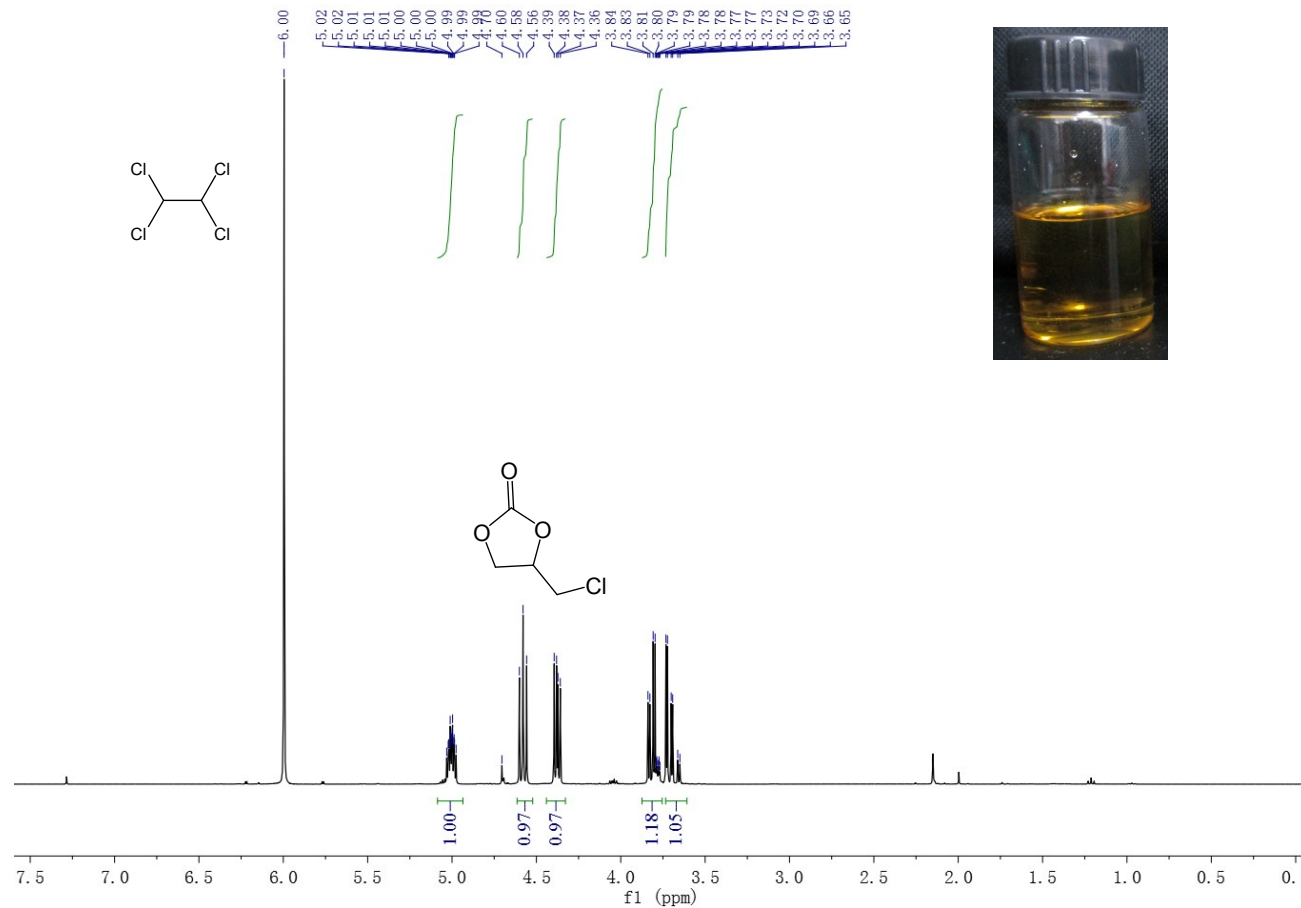
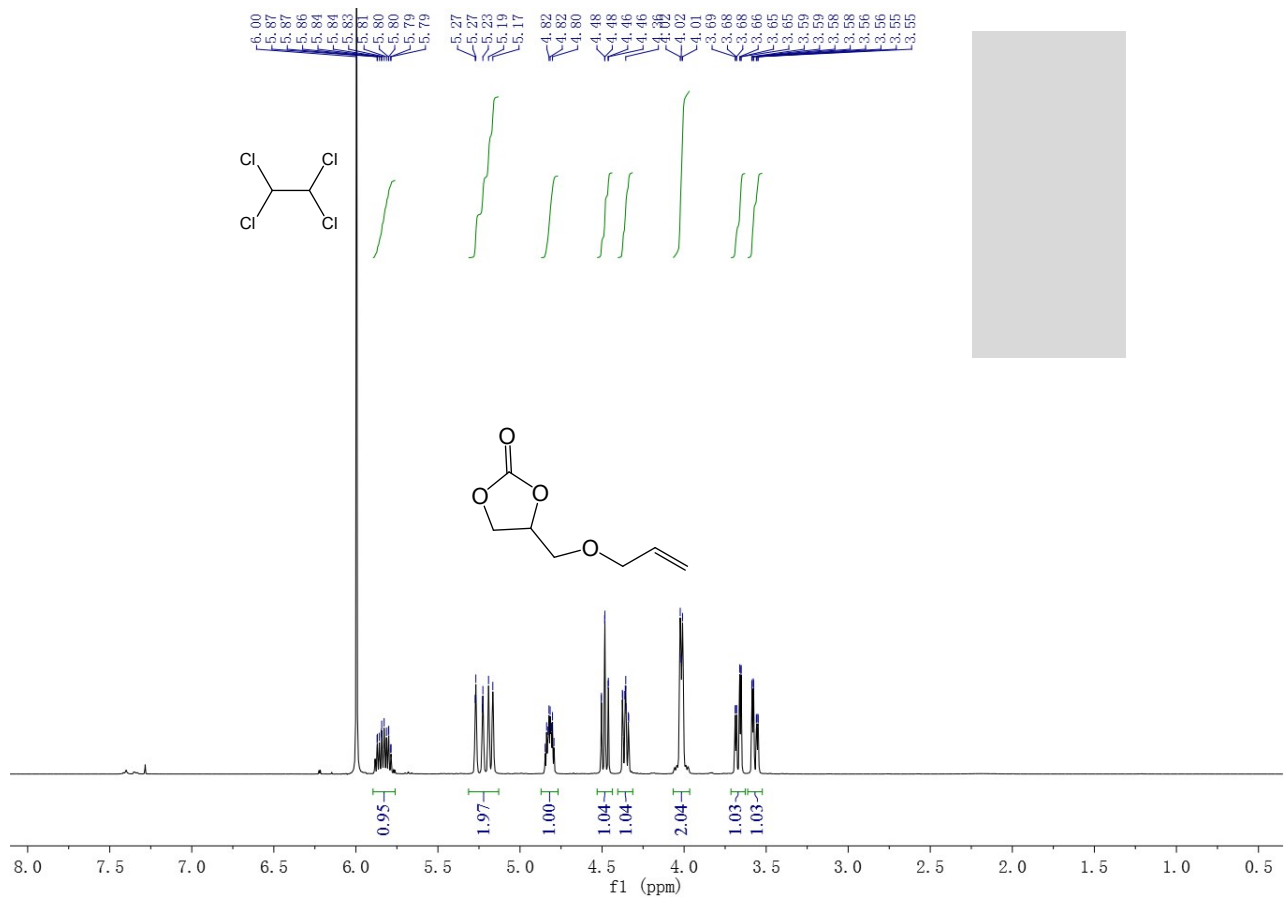


Fig. S17 Typical ^1H NMR method used to calculate the yield of PO.

¹H NMR spectra of the products





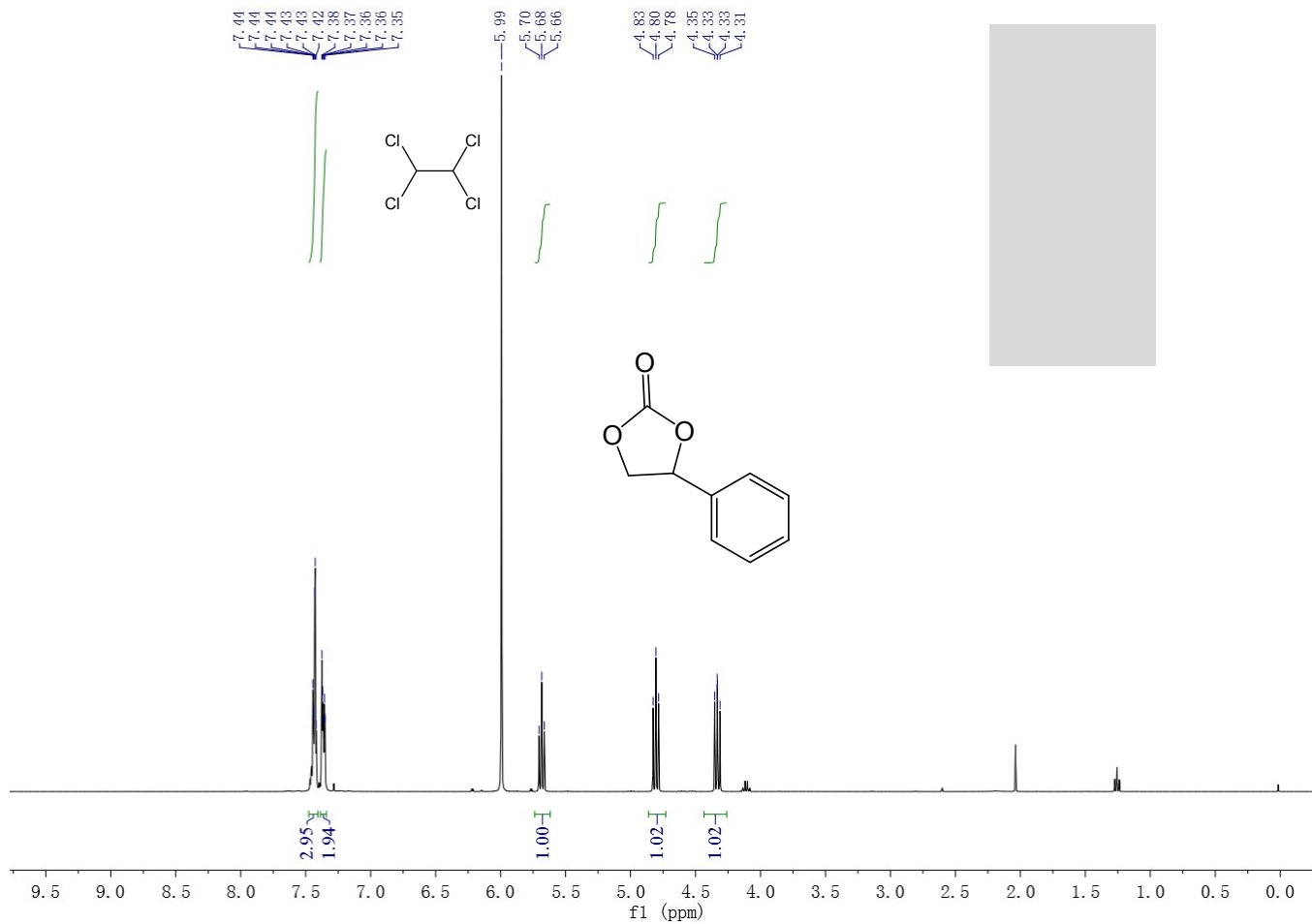


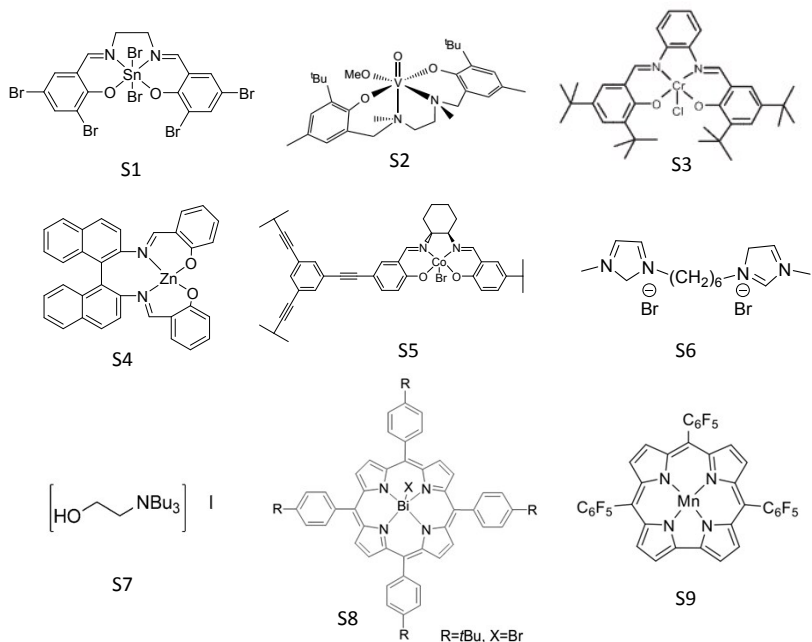
Table S5 Comparison of the Zn@ah-PMF catalyst in the cycloaddition reaction of PO and CO₂ with the reported homogeneous and heterogeneous catalysts.

Category	Catalyst ^[a]	Temp. [°C]	Pressure ^[b] [MPa]	Time [h]	S/C	Conv. [%]	TOF[h ⁻¹]	Ref.
Homogeneous SalenComplexs	S1	120	0.69	5.25	4000-6500	-	531	44
	S2	120	2	5	4000	66	528	45
	S3	75	1.3	2	1500	80	602	46
	S4	100	3.45	2	1000	90	451	47
Heterogeneous SalenComplexs	Co-CMP	100	3	1	205	98.1	201	11
	S5	100	2	16	500	89	20	48
	DVB@ISA	60	1	24	400	99	16.5	49
	Zn@SBMMP	80	2	4	250	97	50.8	50
	Co-MON	60	1	12	2000	75	125	51
	Zn-CMP	120	3	1	2000	55.3	1100	52
Homogeneous Ionic Liquid	[C8-mim] ⁺ [BF4] ⁻	100	14	5 min	60	98	516	53
	[HTEA]I	110	2	6	53	91	8.1	54
	[CBDMAPy]Br	130	2	20 min	100	92	276	55
	S6	110	1.5	2	690	96	331	56
	S7	90	0.5	2	50	92	23	57
Heterogeneous Ionic Liquid	GO-[SmIm]I-40	140	2	4	32	93	7.4	58
	SBA-[V _{0.15} -OH _{0.6}]R ₂ 37	140	2	5	154	95	188	59
	PPh ₃ -ILBr-ZnBr ₂ @POPs	120	3	1	8000	44	3520	13
	PS-MimFeCl ₄	100	8	6	100	77	12.8	60
	PSIL-4	110	6	7	148	97.4	20.6	61
	T-IM	150	1	10	1538	87	134	62
	PDMDBr	110	1	4	77	98.7	19	63
MOF	ZIF-95	80	1.2	2	250	83.2	104	64
	ZnGlu	80	1.2	6	213	99	35	65
	Cu(Hip) ₂ py	120	1.2	6	62	62	6.5	66
	Ni-Salpen-MOF	80	2	4	143	86	31	67
	MOF-5	50	6	4	40	97.6	9.8	68
	UMCM-1-NH ₂	25	1.2	24	156.25	90	5.9	69
	gea-MOF-1	120	2	6	666.7	88	98	16
	Meim-Uio-66	120	0.1	24	192	77	6.2	17
	Tmof-1	25	0.1	48	100	99	2.1	70
	Cu ₆ (μ ₄ -O) ₂ (SO ₄) ₄ (DMA) ₆	25	0.1	24	417	98.2	17.1	71
	In-MOF	80	2	4	769	57.2	110	72
	MIL-101-N(n-Bu)3Br	80	2	8	111	99.1	13.8	73
	Ni-1	40	0.1	40	333	98.4	8.2	74
	[Zn ₆ (TATAB) ₄ (DABCO) ₃ (H ₂ O) ₃] 12DMF 9H ₂ O	100	0.1	16	238	100	15.4	75

(Connected)

Category	Catalyst	Temp. [°C]	Pressure [MPa]	Time [h]	S/C	Conv. [%]	TOF[h ⁻¹]	Ref.
Homogeneous Metalloporphyrin Complexes	S8	90	2	1	100000	37.9	37900	76
	S9	25	0.1	8	2000	55	137	77
Heterogeneous Metalloporphyrin Complexes	Al-HCP	100	3	0.25	20000	18.6	14880	78
	Al-iPOP-2	100	1	4	10000	98	2425	14
	Zn(Por)OP	120	3	2.5	1000	95	1628	79
	Al-CMP	100	3	5	2000	91	364	80
	HUST-1-Co	25	0.1	30	3205	94.6	103	15
Other POPs	Py-Zn@MA	150	2	6	360	96	260	22
	Bp-Zn@MA	100	1	1.5	1160	99	2252	21
	Zn/HAzo-POP-2	100	3	0.5	1872	83	3330	18
	Cu/POP-Bpy	25	0.1	48	200	99	4.1	20
	Zn@AP/HMTA-0.20	100	1	1.5	232	98.6	168.6	19
This work	Zn@ah-PMF	100	2	0.5	11750	79.1	18388	-
	Zn@ah-PMF	25	0.1	55	73800	8.5	114.4	-

[a]The chemical formulas of some catalysts are listed as following.



[b] Pressure refers to the initial CO₂ pressure.

Reference (1-40: main text references, 41-82: electronic supporting information references)

11. Y. Xie, T. T. Wang, X. H. Liu, K. Zou and W. Q. Deng, *Nat. Commun.*, 2013, **4**, 1960.
13. W. Wang, C. Li, L. Yan, Y. Wang, M. Jiang and Y. Ding, *ACS Catalysis*, 2016, **6**, 6091-6100.
14. Y. Chen, R. Luo, Q. Xu, J. Jiang, X. Zhou and H. Ji, *ChemSusChem*, 2017, **10**, 2534-2541.
15. S. Wang, K. Song, C. Zhang, Y. Shu, T. Li and B. Tan, *J. Mater. Chem. A*, 2017, **5**, 1509-1515.
16. V. Guillerm, L. Weselinski, Y. Belmabkhout, A. J. Cairns, V. D'Elia, L. Wojtas, K. Adil and M. Eddaoudi, *Nat. Chem.*, 2014, **6**, 673-680.
17. J. Liang, R. P. Chen, X. Y. Wang, T. T. Liu, X. S. Wang, Y. B. Huang and R. Cao, *Chem. Sci.*, 2017, **8**, 1570-1575.
18. G. Ji, Z. Yang, H. Zhang, Y. Zhao, B. Yu, Z. Ma and Z. Liu, *Angew. Chem.*, 2016, **55**, 9837-9841.
19. F. Liu, K. Huang, Q. Wu and S. Dai, *Adv. Mater.*, 2017, **29**, 1700445.
21. J. Chen, H. Li, M. Zhong and Q. Yang, *Green Chem.*, 2016, **18**, 6493-6500.
22. H. Li, C. Li, J. Chen, L. Liu and Q. Yang, *Chem. Asian J.*, 2017, **12**, 1095-1103.
41. Y. S. Bae, K. L. Mulfort, H. Frost, P. Ryan, S. Punnathanam, L. J. Broadbelt, J. T. Hupp and R. Q. Snurr, *Langmuir*, 2008, **24**, 8592-8598.
42. B. Mu, F. Li and K. S. Walton, *Chem. Commun.*, 2009, 2493-2495.
43. R. Babarao, Z. Hu, J. Jiang, S. Chempath and S. I. Sandler, *Langmuir*, 2007, **23**, 659-666.
44. H. Jing, S. K. Edulji, J. M. Gibbs, C. L. Stern, H. Zhou and S. T. Nguyen, *Inorg. Chem.*, 2004, **43**, 4315-4327.
45. A. I. Elkurtehi and F. M. Kerton, *ChemSusChem*, 2017, **10**, 1249-1254.
46. R. Eberhardt, M. Allmendinger and B. Rieger, *Macromol. Rapid Commun.*, 2010, **24**, 194-196.
47. Y.-M. Shen, W.-L. Duan and M. Shi, *J. Org. Chem.*, 2003, **68**, 1559-1562.
48. M. H. Alkordi, Ł. J. Weseliński, V. D'Elia, S. Barman, A. Cadiau, M. N. Hedhili, A. J. Cairns, R. G. AbdulHalim, J.-M. Basset and M. Eddaoudi, *J. Mater. Chem. A*, 2016, **4**, 7453-7460.
49. R. Luo, Y. Chen, Q. He, X. Lin, Q. Xu, X. He, W. Zhang, X. Zhou and H. Ji, *ChemSusChem*, 2017, **10**, 1526-1533.
50. S. Bhunia, R. A. Molla, V. Kumari, S. M. Islam and A. Bhaumik, *Chem. Commun.*, 2015, **51**, 15732-15735.
51. J. Chun, S. Kang, N. Kang, S. M. Lee, H. J. Kim and S. U. Son, *J. Mater. Chem. A*, 2013, **1**, 5517-5523.
52. Y. Xie, T. T. Wang, R. X. Yang, N. Y. Huang, K. Zou and W. Q. Deng, *ChemSusChem*, 2014, **7**, 2110-2114.
53. H. Kawanami, A. Sasaki, K. Matsui and Y. Ikushima, *Chem. Commun.*, 2003, 896-897.
54. M. Liu, X. Li, L. Liang and J. Sun, *J. CO₂ Util.*, 2016, **16**, 384-390.
55. X. Meng, H. He, Y. Nie, X. Zhang, S. Zhang and J. Wang, *ACS Sustainable Chem. Eng.*, 2017, **5**, 3081-3086.
56. M. Liu, L. Liang, T. Liang, X. Lin, L. Shi, F. Wang and J. Sun, *J. Mol. Catal. A-Chem.*, 2015, **408**, 242-249.
57. H. Büttner, K. Lau, A. Spannenberg and T. Werner, *ChemCatChem*, 2015, **7**, 459-467.
58. J. Zhu, Y. Gu, J. Wu, X. Zhu, B. Xue and Y. Li, *Catal. Lett.*, 2016, **147**, 335-344.
59. S. Jayakumar, H. Li, Y. Zhao, J. Chen and Q. Yang, *Chem. Asian J.*, 2017, **12**, 577-585.
60. J. Gao, Q.-W. Song, L.-N. He, C. Liu, Z.-Z. Yang, X. Han, X.-D. Li and Q.-C. Song, *Tetrahedron*, 2012, **68**, 3835-3842.
61. Y. Xie, Z. Zhang, T. Jiang, J. He, B. Han, T. Wu and K. Ding, *Angew. Chem.*, 2007, **119**, 7393-7396.

62. H. C. Cho, H. S. Lee, J. Chun, S. M. Lee, H. J. Kim and S. U. Son, *Chem. Commun.*, 2011, **47**, 917-919.
63. X. Wang, Y. Zhou, Z. Guo, G. Chen, J. Li, Y. Shi, Y. Liu and J. Wang, *Chem. Sci.*, 2015, **6**, 6916-6924.
64. K. M. Bhin, J. Tharun, K. R. Roshan, D.-W. Kim, Y. Chung and D.-W. Park, *J. CO₂ Util.*, 2017, **17**, 112-118.
65. A. C. Kathalikkattil, R. Babu, R. K. Roshan, H. Lee, H. Kim, J. Tharun, E. Suresh and D.-W. Park, *J. Mater. Chem. A*, 2015, **3**, 22636-22647.
66. A. C. Kathalikkattil, D.-W. Kim, J. Tharun, H.-G. Soek, R. Roshan and D.-W. Park, *Green Chem.*, 2014, **16**, 1607-1616.
67. Y. Ren, X. Cheng, S. Yang, C. Qi, H. Jiang and Q. Mao, *Dalton Trans.*, 2013, **42**, 9930-9937.
68. J. Song, Z. Zhang, S. Hu, T. Wu, T. Jiang and B. Han, *Green Chem.*, 2009, **11**, 1031-1036.
69. R. Babu, A. C. Kathalikkattil, R. Roshan, J. Tharun, D.-W. Kim and D.-W. Park, *Green Chem.*, 2016, **18**, 232-242.
70. G. Zhang, G. Wei, Z. Liu, S. R. J. Oliver and H. Fei, *Chem. Mater.*, 2016, **28**, 6276-6281.
71. S.-S. Yu, X.-H. Liu, J.-G. Ma, Z. Niu and P. Cheng, *J. CO₂ Util.*, 2016, **14**, 122-125.
72. L. Liu, S. M. Wang, Z. B. Han, M. Ding, D. Q. Yuan and H. L. Jiang, *Inorg. Chem.*, 2016, **55**, 3558-3565.
73. D. Ma, B. Li, K. Liu, X. Zhang, W. Zou, Y. Yang, G. Li, Z. Shi and S. Feng, *J. Mater. Chem. A*, 2015, **3**, 23136-23142.
74. Z. Zhou, L. Yang, Y. Wang, C. He, T. Liu and C. Duan, *RSC Adv.*, 2016, **6**, 108010-108016.
75. Y.-H. Han, Z.-Y. Zhou, C.-B. Tian and S.-W. Du, *Green Chem.*, 2016, **18**, 4086-4091.
76. J. Peng, Y. Geng, H.-J. Yang, W. He, Z. Wei, J. Yang and C.-Y. Guo, *Mol. Catal.*, 2017, **432**, 37-46.
77. M. Tiffner, S. Gonglach, M. Haas, W. Schofberger and M. Waser, *Chem. Asian J.*, 2017, **12**, 1048-1051.
78. Y. Chen, R. Luo, Q. Xu, W. Zhang, X. Zhou and H. Ji, *ChemCatChem*, 2017, **9**, 767-773.
79. A. Chen, Y. Zhang, J. Chen, L. Chen and Y. Yu, *J. Mater. Chem. A*, 2015, **3**, 9807-9816.
80. X. Sheng, H. Guo, Y. Qin, X. Wang and F. Wang, *RSC Adv.*, 2015, **5**, 31664-31669.
81. B. Delley, *J. Chem. Phys.*, 1990, **92**, 508-517.
82. B. Delley, *J. Chem. Phys.*, 2000, **113**, 7756-7764.

Appendix 1 The program code of IAST

PROGRAM IAST

```
*****  
! This program is used to predict binary mixture adsorption from the  
! experimental pure-gas isotherms  
*****  
  
IMPLICIT NONE  
REAL(8),DIMENSION(1:2) :: y, qm1, b1, n1, qm2, b2, n2  
REAL(8) bisection  
INTEGER i, n  
REAL(8),DIMENSION(1:100) :: P, x1, x2, S  
  
*****  
! This section is used to read the parameters of the non-linear curve fit  
! for the pure isotherms of CO2 and N2 at 273 K.  
*****  
  
OPEN (UNIT=10,FILE="d:\INPUT.txt", STATUS="UNKNOWN")  
READ(10,*) n  
READ(10,*) (y(i),i=1,2) !for flue gas, y(1)=0.15,y(2)=0.85; for ideal gas, y(1)=y(2)=0.5  
READ(10,*) (P(i),i=1,n)  
READ(10,*) (qm1(i),i=1,2)  
READ(10,*) (b1(i),i=1,2)  
READ(10,*) (n1(i),i=1,2)  
READ(10,*) (qm2(i),i=1,2)  
READ(10,*) (b2(i),i=1,2)  
READ(10,*) (n2(i),i=1,2)  
CLOSE(10)  
*****  
  
DO i=1,n  
    x1(i)=bisection(P(i),qm1,b1,n1,qm2,b2,n2,y)  
    x2(i)=1-x1(i)  
END DO  
  
DO i=1,n  
    S(i)=(x1(i)/y(1))/(x2(i)/y(2)) !To calculate the selectivity  
END DO  
  
OPEN (UNIT=20,FILE="d:\OUTPUT_DSLF.txt", STATUS="UNKNOWN")  
DO i=1,n  
    WRITE(20,100) P(i), S(i), x1(i), x2(i), y(1), y(2)
```

```

END DO
100  format(10f15.6)
CLOSE(20)
END

!*****
! This Section is used to calculate the root of equation "f" by the method
! of bisection and the function is named as "bisection"
!*****

FUNCTION bisection(P,qm1,b1,n1,qm2,b2,n2,y)
IMPLICIT NONE
REAL(8),DIMENSION(1:2) :: qm1, b1, n1, qm2, b2, n2, y
REAL(8) lt, rt, mi, f, P, bisection
lt=0.0
rt=1.0
DO WHILE (ABS(rt-lt)>1E-10)
    mi=(lt+rt)/2
    IF (f(P,qm1,b1,n1,qm2,b2,n2,y,lt)*f(P,qm1,b1,n1,qm2,b2,n2,y,mi)<0) THEN
        rt=mi
    ELSE
        lt=mi
    END IF
END DO
bisection=mi
END FUNCTION bisection
!*****



!*****
! The Function is the equation from IAST theory, and the pure-gas
! isotherm is fitted with dual-site Langmuir-Freundlich model.
! *****

FUNCTION f(P,qm1,b1,n1,qm2,b2,n2,y,x1)
IMPLICIT NONE
REAL(8),DIMENSION(1:2) :: qm1, b1, n1, qm2, b2, n2, y
REAL(8) P, x1, f, f1, f2
f1=qm1(1)*n1(1)*LOG(1+b1(1)*(P*y(1)/x1)**(1/n1(1)))+qm2(1)*n2(1)*LOG(1+b2(1)*(P*y(1)/x1)**(1/n2(1)))
f2=qm1(2)*n1(2)*LOG(1+b1(2)*(P*y(2)/(1-x1))**(1/n1(2)))+qm2(2)*n2(2)*LOG(1+b2(2)*(P*y(2)/(1-
x1))**(1/n2(2)))
f=f1-f2
END FUNCTION f
!*****

```

Appendix 2 The input value and the predicted results of ideal gas and flue gas via IAST

(1) The input value.

26# This is the number of pressure value.

0.15, 0.85# This is the molar fraction of CO₂ and N₂ in bulk phase. 0.15/0.85 is the ratio of flue gas, and 0.5/0.5 is the ratio of ideal gas.

3.05E-04, 5.08E-04, 7.11E-04, 9.13E-04, 0.00102, 0.00521, 0.01029, 0.01531, 0.01787, 0.02042, 0.02545, 0.03051, 0.03558, 0.04066, 0.04572, 0.05078, 0.05586, 0.06093, 0.06599, 0.07106, 0.07612, 0.08118, 0.08625, 0.09132, 0.09638, 0.10096# This is the selected pressure value, and the unit is MPa.

1.88361, 1.01283# This is the fitting parameter q_{m,1} of CO₂ and N₂, respectively.

2.04164, 0.33765# This is the fitting parameter b₁ of CO₂ and N₂, respectively

0.84167, 1.18592# This is the fitting parameter n₁ of CO₂ and N₂, respectively

0.96608, 1.01266# This is the fitting parameter q_{m,2} of CO₂ and N₂, respectively

11.28204, 0.33652# This is the fitting parameter b₂ of CO₂ and N₂, respectively

1.36777, 1.18589# This is the fitting parameter n₂ of CO₂ and N₂, respectively

(2) The output results for ideal gas via IAST.

Pressure (MPa)	Selectivity	x_{CO_2}	x_{N_2}	y_{CO_2}	y_{N_2}
0.000305	101.6569	0.990259	0.009741	0.5	0.5
0.000508	94.89442	0.989572	0.010428	0.5	0.5
0.000711	90.65712	0.98909	0.01091	0.5	0.5
0.000913	87.60955	0.988715	0.011285	0.5	0.5
0.00102	86.28583	0.988543	0.011457	0.5	0.5
0.00521	68.40017	0.985591	0.014409	0.5	0.5
0.01029	61.61455	0.984029	0.015971	0.5	0.5
0.01531	57.79085	0.982991	0.017009	0.5	0.5
0.01787	56.32932	0.982557	0.017443	0.5	0.5
0.02042	55.08075	0.982169	0.017831	0.5	0.5
0.02545	53.04622	0.981497	0.018503	0.5	0.5
0.03051	51.39798	0.980915	0.019085	0.5	0.5
0.03558	50.02234	0.980401	0.019599	0.5	0.5
0.04066	48.84612	0.979938	0.020062	0.5	0.5
0.04572	47.82781	0.97952	0.02048	0.5	0.5
0.05078	46.92997	0.979136	0.020864	0.5	0.5
0.05586	46.12645	0.97878	0.02122	0.5	0.5
0.06093	45.40514	0.978451	0.021549	0.5	0.5
0.06599	44.75255	0.978143	0.021857	0.5	0.5
0.07106	44.15602	0.977855	0.022145	0.5	0.5
0.07612	43.60991	0.977583	0.022417	0.5	0.5
0.08118	43.10657	0.977328	0.022672	0.5	0.5
0.08625	42.63985	0.977085	0.022915	0.5	0.5
0.09132	42.20639	0.976855	0.023145	0.5	0.5
0.09638	41.80332	0.976637	0.023363	0.5	0.5
0.10096	41.46132	0.976449	0.023551	0.5	0.5

(3) The output results for flue gas.

Pressure (MPa)	Selectivity	x_{CO_2}	x_{N_2}	y_{CO_2}	y_{N_2}
0.000305	118.821	0.95448	0.04552	0.15	0.85
0.000508	110.9571	0.951411	0.048589	0.15	0.85
0.000711	106.0476	0.949275	0.050725	0.15	0.85
0.000913	102.5279	0.947625	0.052375	0.15	0.85
0.00102	101.0025	0.946876	0.053124	0.15	0.85
0.00521	80.70337	0.934391	0.065609	0.15	0.85
0.01029	73.20708	0.928155	0.071845	0.15	0.85
0.01531	69.02988	0.924137	0.075863	0.15	0.85
0.01787	67.43834	0.922486	0.077514	0.15	0.85
0.02042	66.07929	0.921018	0.078982	0.15	0.85
0.02545	63.86251	0.918499	0.081501	0.15	0.85
0.03051	62.06058	0.916331	0.083669	0.15	0.85
0.03558	60.54894	0.914421	0.085579	0.15	0.85
0.04066	59.24819	0.912706	0.087294	0.15	0.85
0.04572	58.11387	0.911154	0.088846	0.15	0.85
0.05078	57.10579	0.909727	0.090273	0.15	0.85
0.05586	56.19599	0.908399	0.091601	0.15	0.85
0.06093	55.37199	0.907163	0.092837	0.15	0.85
0.06599	54.61965	0.906004	0.093996	0.15	0.85
0.07106	53.92544	0.904909	0.095091	0.15	0.85
0.07612	53.28377	0.903874	0.096126	0.15	0.85
0.08118	52.68652	0.90289	0.09711	0.15	0.85
0.08625	52.1272	0.90195	0.09805	0.15	0.85
0.09132	51.60248	0.901052	0.098948	0.15	0.85
0.09638	51.10955	0.900193	0.099807	0.15	0.85
0.10096	50.68719	0.899445	0.100555	0.15	0.85